Long-term (>90 years) wastewater irrigation effect on the pore characteristics and stability of soil aggregates

Ceres Perezvargas y Castor, Alfonso Gastélum-Strozzi, Stéphane Sammartino, Eric Michel, Jérôme Vicente, Blanca Prado

HAL Id: hal-04174934
https://hal.inrae.fr/hal-04174934

Submitted on 1 Aug 2023

Long-term (>90 years) wastewater irrigation effect on the pore characteristics and stability of soil aggregates

Ceres Perezvargas y Castor [a], Alfonso Gastélum-Strozzi [b], Stéphane Sammartino [c], Eric Michel [d], Jérôme Vicente [e], Blanca Prado [f,*]

[a] Posgrado en Ciencias de La Tierra, Universidad Nacional Autónoma de México, Ciudad Universitaria, Mexico City, Avenida Universidad 3000, Coyoacán, Ciudad de México 04510, Mexico
[b] Instituto de Ciencias Aplicadas y Tecnología, Universidad Nacional Autónoma de México, Ciudad Universitaria, Mexico City, Avenida Universidad 3000, Coyoacán, Ciudad de México 04510, Mexico
[c] EMMAH, Avignon Université, INRAE, 84000 Avignon, France
[d] EMMAH, INRAE, Avignon Université, 84000 Avignon, France
[e] Aix Marseille Univ, CNRS, IUSTI, Marseille, France
[f] Instituto de Geología, Universidad Nacional Autónoma de México, Ciudad Universitaria, Mexico City, Avenida Universidad 3000, Coyoacán, Ciudad de México 04510, Mexico

ARTICLE INFO

ABSTRACT

Wastewater (WW) agricultural irrigation is becoming a common practice as an alternative to water scarcity. However, WW irrigation may affect the soil structure at different hierarchical levels. This issue was tackled by evaluating the long-term (>90 years) WW irrigation effects on soil structure. Samples of Ap and Ah horizons from eight rainfed and eight WW-irrigated plots were collected for physicochemical characterization. Undisturbed samples were analyzed for aggregate stability, and the pore space of small macroaggregates (0.5–1 mm) from Ah horizons of three rainfed and three WW-irrigated plots was analyzed by x-ray microtomography. Long-term WW-irrigated plots had higher contents of C (Ap = 2.54%; Ah = 1.64%) and N (Ap = 0.24%; Ah = 0.16%) compared to rainfed soils, as well as higher aggregates stability (mean weight diameter = 23.6 mm, p = 0.001). However, soil organic matter accumulation was not the main driver of the higher aggregate stability in WW-irrigated soils (Spearman correlation coefficients of 0.467 and 0.476 for organic C and total N, respectively). It was proposed that a combination of factors including SOM and easily degradable OM (C/N = 2.10) input from WW was the reason for this higher stability. The results did not allow one to conclude on the long-term effect of WW irrigation on the microstructural pore space because the scatter in the data of the rainfed samples was high. Considering a higher number of samples may address this problem. Nevertheless, the findings of this research improve our understanding of the effects of WW irrigation on soil structure and provide a better assessment of the benefits and risks associated with this practice.

1. Introduction

The three-dimensional organization of the soil solids, called "soil structure" – and its reciprocal, the pore space – controls water movement, solute transport, carbon storage, aeration, and organic matter turnover (Bronick and Lal, 2005; Schlüter et al., 2020). Several factors affect the stability of this structure. Cation composition, clay mineralogy, and organic matter are often mentioned as intrinsic factors mainly involved in flocculation and cementation processes. External factors include biological activity, as well as soil management: tillage and irrigation practices (including water quality) can both improve or damage the stability of soil structure (Amézketa, 1999).

WW irrigation has become a common agricultural practice around the world to mitigate the effects of water scarcity (Hettiarachchi and Ardakanian, 2016; Valipour and Singh, 2016). Nevertheless, WW contains sodium salts, organic matter, and suspended solids that may affect the soil structure. It has been reported that suspended solids contained in wastewater can be retained in the soil pore space and decrease the soil porosity and hydraulic conductivity of wastewater-irrigated soils (Gharaibeh et al., 2007; Schacht and Marschner, 2015; Müller et al.,

Table 1
Physichochemical characteristics of wastewater.

DOC (mg L^{-1})	N-NO$_3$ (mg L^{-1})	N-NH$_4^+$ (mg L^{-1})	pH	Turbidity (NTU)	EC (mS cm^{-1})	Na$^+$ (meq L^{-1})	Ca^{2+} (meq L^{-1})	Mg^{2+} (meq L^{-1})	SAR[a]
77.04	<DL[b]	36.60	7.54	ND[c]	1.52	7.85	1.76	1.99	5.73

[a] < DL: Under detection limit. DL for N-NO$_3$ = 0.1 mg L^{-1}; ND: Not determined.
[b] SAR: sodium adsorption ratio. SAR = [Na$^+$]/ (([Ca^{2+}] + [Mg^{2+}])/2) ̇0.5.
[c] ND: Not determined.

2012). Furthermore, the soil salinity induced by WW irrigation has been reported to reduce the stability of soil aggregates (Schacht and Marschner, 2015). However, the organic matter contained in wastewater has also been found to increase the soil organic carbon (SOC) content and the aggregate stability in soils irrigated for 5 and 15 years with olive mill WW, compared to freshwater-irrigated soils (Mahmoud et al., 2012).

These contrasting observations suggest that the long-term effects of wastewater irrigation on soil structure are not fully understood. This prevents a proper assessment of the benefits and risks associated with this practice. This lack of understanding probably stems from the strong dependency of these effects on both WW quality and soil properties (Schacht and Marschner, 2015), besides the fact that, to date, studies investigating the impacts of long-term irrigation with WW on soil structure are scarce (Levy and Assouline, 2010).

X-ray microtomography is a non-destructive technique that has been extensively used to characterize the structure of soils at the column scale (Dal Ferro et al., 2012; Pituello et al., 2016; Prado et al., 2016; Duwig et al., 2019), and at the aggregate scale (Wang et al., 2012; Dal Ferro et al., 2013; Menon et al., 2020; Zhao et al., 2020) to compare various soil management practices including land use, the impact of macrofauna abundance, the impact of fertilization and residue management on soil porosity. To the best of our knowledge, only two X-ray tomography studies focused on the impact of WW on soil structure: Leuther et al. (2019) studied WW-irrigated soils for 10–30 years and found that the irrigation favors the development of a connected macropore network, as well as that fine textured soil was much more resistant to soil alteration by WW-irrigation than coarser soil. Marchuk and Marchuk (2018) focused on the impact of the application of potassium in soil porosity. In both cases, the analysis was made at the soil column scale.

Given the above, the aim was to understand how >90 years under WW irrigation may affect the soil structure of a cultivated soil (corn – alfalfa rotation), from the aggregates and the pore space perspectives. From the aggregate perspective, we hypothesized that the increasing soil organic carbon in WW-irrigated soils would lead to greater aggregate stability compared to soils that had never been irrigated with WW (rainfed soils). From the pore space perspective, we hypothesized that: i) the organic matter accumulated in the WW-irrigated soils would reduce their bulk density, and consequently increase their total porosity, compared to rainfed ones; ii) the input of sodium salts and suspended solids in the WW affluent would increase the proportion of small pores and decrease the proportion of large pores in the WW-irrigated soils compared to the rainfed ones.

To test these hypotheses, we analyzed the aggregate stability and microstructural pore space –determined from X-ray microtomography– of soil samples taken from fields that had never been irrigated with WW and fields that had been irrigated with WW for >90 years. We finally aimed to integrate both perspectives to completely understand the long-term WW-irrigation effect on soil structure.

2. Materials and methods

2.1. Studied zone

The Mezquital Valley is a region in the state of Hidalgo, Mexico, 60–80 km north of Mexico City. It has a semiarid climate with a rainy season in summer, between June and September. Its mean annual temperature ranges from 15 to 17 °C (González-Méndez et al., 2017). There are three different soil types in the Mezquital Valley: Vertisols, Phaeozems, and Leptosols (Siebe et al. 2016). The first two represent >65% of the valley surface. Rainfed maize agriculture gradually expanded in the valley before the Spanish conquest (1521) until the 19th century, when crop irrigation with Mexico City wastewater officially started (Sánchez-González et al., 2017). The WW-irrigated surface now reaches approximately 90,000 ha (Siebe et al., 2016). In the Mezquital Valley plots coexist from 0 (rainfed) to several years of WW irrigation. In the wastewater-irrigated plots, maize and alfalfa are rotated in cycles of two and three years, respectively; while rainfed plots are used for maize growing in summer and kept fallow during the dry season (Lüneberg-Rodríguez, 2018). In both kinds of plots (rainfed and long-term WW-irrigated soils) tillage is practiced to a depth of 20 cm to prepare the soil for sowing. In the Mezquital Valley, the lands are inherited from parents to children, so the information on the number of years under irrigation with WW, as well as the land use conditions prior to wastewater-irrigation, are given by the farmers.

It has been documented that the SOC concentration in the Mezquital Valley increases with the duration of WW irrigation and reaches a maximum after 40 years. Then, the SOC concentration remains constant for at least 50 years with the same management (Sánchez-González et al., 2017). Furthermore, although clay mineralogy in the valley changes from smectite in the rainfed irrigated plots to illite/smectite in the plots irrigated with WW for 90 years (Sánchez-González, 2018), the soil texture is similar between the plots with different irrigation systems. The physicochemical properties of wastewater at the sampling moment are given in Table 1, but historical compositions are also presented in Table S1.

2.2. Sampling and experimental design

We sampled sixteen plots with vertic phaeozems (vertic haplustol in USDA soil taxonomy) between October 2019 and February 2020: eight rainfed (R0) and eight that had been irrigated with WW for at least 90 years (R90). This duration of WW irrigation was determined by orally interviewing the plot owners about the year WW irrigation started on their land. Before that moment, between 1922 and 1927, the fields were used for the intensive production of maize. At the time of sampling, WW-irrigated plots were cultivated with maize. Rainfed plots were under fallow.

In each plot, a superficial tilled horizon (Ap) and the underlying structured horizon (Ah) (from about 30–35 cm depth) were sampled. From each horizon, an unaltered soil column was sculpted (10 cm in diameter and 10 cm in height) and carefully transported to the laboratory. This column was used for aggregate stability tests. Bulk samples were also taken for physicochemical characterization. The samples were grouped into four treatments: 1) rainfed surficial (R0-Ap), 2) rainfed sub-surficial (R0-Ah), 3) WW-irrigated surficial (R90-Ap), and 4) WW-irrigated sub-surficial (R90-Ah). A total of 32 samples were analyzed, with eight samples in each treatment.

2.3. Soil physicochemical characterization

Electrical conductivity and pH were measured in triplicate in a 1:5

Table 2
Physicochemical characteristics.

Treatment[d]	Organic C %	Inorganic C %	Total N %	Clay %	pH	EC µS cm-1	Na$^+$ meq L-1	BD g cm-3	Total porosity %
R0-Ap	1.45 (0.49)e	0.06 (0.10)	0.14 (0.04)	41.05 (8.24)	7.75 (0.28)	374.08 (210.29)	0.24 (0.09)	1 (0.08)	62.33 (3.21)
R0-Ah	1.02 (0.32)	0.05 (0.05)	0.10 (0.02)	40.81 (10.20)	8.09 (0.11)	303.83 (96.50)	0.63 (0.60)	0.98 (0.09)	63.10 (3.48)
R90-Ap	2.54 (0.39)	0.10 (0.14)	0.24 (0.03)	42.19 (8.28)	7.51 (0.45)	604.17 (151.69)	3.38 (0.77)	0.93 (0.07)	64.76 (2.44)
R90-Ah	1.64 (0.34)	0.07 (0.06)	0.16 (0.04)	40.89 (8.82)	7.85 (0.44)	426.38 (57.48)	3.13 (0.53)	1.04 (0.12)	60.68 (4.57)

dR0 (rainfed) and R90 (WW irrigated) samples correspond to different plots and were taken in the same season.
eMean (standard deviation) of each group of data.

Table 3
Aggregates classes.

Class	Class name	Sieve diameter (mm)
"A"	Mega aggregates	2
"B"	Large macro aggregates	1
"C"	Small macro aggregates	0.25
"D"	Micro aggregates	0.053
"E"	Mineral fraction (silt + clay)	—

suspension with deionized water (Hanna Instruments edge® multiparameter HI2020, probes SHI663100 and SHI12300). After this measurement, the supernatant was filtered through a 0.45 µm nylon filter and analyzed for major cations (Leuther et al., 2019). The use of water as a solvent allows the evaluation of the soluble fraction and avoids interferences in the determination by ion chromatography. The latter technique was used to determine major cations using a Waters 1525 chromatograph equipped with a binary pump, an autosampler (717), and an electric conductivity detector (432). Cations were quantified using as stationary phase a Metrosep C4 column (Metrohm) of 4×100 mm. The mobile phase was a 1.9 mM HNO_3 solution with 0.8 mM dipicolinic acid in isocratic mode and a flux of 0.9 ml min^{-1} (Hernández-Martínez et al., 2018).

The bulk soil was air–dried, grounded in an agate mortar, and sieved through a 0.25 mm mesh for total N as well as total and organic C analysis (Thermo Scientific Flash 2000 elemental analyzer) (Abbruzzini et al., 2022). Organic C was measured after removing carbonates with HCl (Harris et al., 2001).

For particle size distribution, bulk soil was air–dried and sieved through a 2 mm mesh. Two 50 g samples were weighted, and their organic matter and dithionite-extractable Fe were eliminated. One of the samples was dried at 105 °C to determine the dry soil weight, while the other was measured by using an automated texture analyzer PARIO Soil Particle Analyzer© from METER Group, which calculates particle size distribution from pressure in the suspension at a given depth (Durner et al., 2017).

Bulk density (BD) was determined by using 100 cm^3 cores collected with standardized steel cylinders. The total porosity of the bulk soil was calculated assuming a solid density of 2.65 g cm^{-3} as indicated in Eq. (1).

$$\text{Total porosity (\%)} = 1 - (BD/2.65) * 100 \tag{1}$$

Physicochemical characteristics of each of the six studied plots are given in Table S2 to S5, while means of the studied soils (grouped by treatment, rainfed and WW-irrigated soils) are given in Table 2.

2.4. Aggregates stability and sand correction

With the soil at field capacity, the larger clods in the unaltered soil columns were hand-broken following their natural rupture planes, until aggregates of 10 mm in diameter were obtained. Only the size of the first 10 mm aggregate was measured. The subsequent aggregates were visually compared to the first one. Then, 25 g of such aggregates were wet-sieved (Díaz-Zorita et al., 2002; Almajmaie et al., 2017) by loading

them at the top of a stack of sieves with descending aperture order (2000 > 1000 > 250 > 53 µm) resulting in five aggregates classes (Table 3). The stack was fitted in an automatic sieving apparatus. The stack was carefully submerged in a pail containing enough distilled water to fully cover the sample, without spilling inwards from the upper edge of the top–most sieve and was sieved for 5 min at a speed of 23 cycles/minute with a stroke amplitude of 3 cm. The aggregates retained by each sieve were recovered by carefully washing them into a previously labeled and weighted aluminum tray, after which they were dried at 105 °C and weighted. This analysis was performed in triplicate for each studied sample. Approximately 5 g of fresh 10 mm aggregates were dried at 105 °C (in triplicate) to determine their moisture content. This value was used to compute the total dry weight of soil loaded into the sieve stack (W_{DS}). The relative weight of each aggregate class (W_i) was calculated by dividing its dry weight by W_{DS}.

For every sample, one of the triplicates was used to calculate the correction factor for sand content following a modification to the method proposed by Moritsuka et al. (2015). Briefly, after recording the W_i for each aggregate class, the aggregates were carefully transferred into a previously weighted nylon cloth with a 50 µm pore size. The cloth was sealed with a rubber band and washed with running water until the effluent was clear. The sands remaining in the cloth were air dried to constant weight, and the cloth weight was subtracted to obtain the mass of sand present in the aggregate class. This value was divided by the mass initially transferred onto the cloth (approximately equal to W_i) to get the mass of sand relative to the mass of aggregates, i.e., the sand fraction, in the aggregate class (S_i). The S_i was then used to calculate the water–stable aggregates of every class (WSA_i) as indicated in Eq. (2), where W_i is the mean for the three replicates.

$$WSA_i = W_i - (S_i * W_i) \tag{2}$$

Then, the water–stable aggregates distribution ($WSAD_i$) was calculated by dividing the WSA_i by the total sum of the WSA_i values obtained for each sample, as indicated in Eq. (3), where n is the number of analyzed aggregates classes. The results were expressed as cumulative graph bars.

$$WSAD_i(\%) = \frac{WSA_i}{\sum_{i=1}^{n} WSA_i} * 100 \tag{3}$$

Furthermore, the mean weighted diameter (MWD) of each sample, an indicator of the soil aggregates' stability, was calculated following Eq. (4)., where n is the number of analyzed aggregates classes, and X_i is the mean diameter of the aggregates class (mm), i.e., the mean of the upper and lower sieves diameter (Díaz-Zorita et al., 2002). The MWD was used as a descriptor of the macrostructure.

$$MWD\ (mm) = \sum_{i=1}^{n} X_i * WSA_i \tag{4}$$

2.5. Microtomography measurements and analysis

2.5.1. Procurement of macro aggregates and image acquisition

Small macroaggregates between 0.5 and 1 mm in diameter were obtained by wet sieving as previously described from the sub-surficial

Table 4

Kruskal-Wallis test for physicochemical characteristics.

	R0-Ap[f] Median (rank)	R0-Ah[g] Median (rank)	R90-Ap[h] Median (rank)	R90-Ah[i] Median (rank)	H	p
Organic C	1.17 (1.13)	0.91 (0.94)	2.58 (1.16)	1.57 (0.94)	21.08	<0.001
Total N	0.12 (0.11)	0.09 (0.05)	0.23 (0.09)	0.14 (0.09)	22.44	<0.001
Na$^+$	0.25 (0.21)	0.39 (1.75)	3.41 (2.00)	3.24 (1.57)	24.17	<0.001
EC	307.170 (652.00)	301.84 (303.66)	585.34 (457.67)	441 (163.33)	16.04	0.001
pH	7.81 (0.79)	8.15 (0.95)	7.62 (1.27)	7.90 (1.33)	8.414	0.038
Bulk density	1.01 (0.26)	0.94 (0.23)	0.92 (0.19)	1.02 (0.27)	4.94	0.176
Total porosity	61.83 (9.94)	64.53 (8.93)	65.35 (7.17)	61.58 (10.18)	4.65	0.199

[f] R0-Ap: rainfed surficial horizon.
[g] R0-Ah: rainfed sub surficial horizon.
[h] R90-Ap: WW-irrigated surficial horizon.
[i] R90-Ah: WW-irrigated sub surficial.

horizon of three rainfed and three long-term WW irrigated plots randomly selected. Only sub-surface horizons were considered for microtomography to avoid the influence of tillage. The aggregates class was chosen to have the lowest field of view (in the order of 1 mm) while assuring that macroaggregates were analyzed (according to Elliot and Coleman (1988) macroaggregates contain the whole range of porosity). The macroaggregates were air-dried until a constant weight was reached. Three aggregates of each sample, separated and immobilized by polyurethane foam, were then carefully inserted into glass capillaries (1.1–mm inner diameter). The capillaries were sealed to maintain them at a constant hydric state. Image acquisition was carried out at IUSTI laboratory, Marseille, France with an ad hoc microtomography RX Solutions ^{TM}; operating with a 70 kV x-ray source – taking between 1315 and 1560 2D images for the sample situated on a rotating sample holder (Wildenschild and Sheppard, 2013). The acquisition of these images took approximately 2.5 h per sample. These 2D images were converted into a stack of 3D images with a voxel size of 2.4–μm. In these stacks, the voxel grey level is proportional to the density of the material (the brighter the voxels, the higher the material density).

2.5.2. Image processing

A segmentation algorithm was implemented in ImageJ to measure the pore space contained in the aggregates. First, a simple histogram thresholding was used to discard all the voxels belonging to the glass capillary and foam. The second step was to separate each aggregate in the image stack (volume). For this, the volume was first binarized into voxels that were soil (1) and the rest (0). Next, the binarized volume was eroded by a morphological operator with an ellipsoidal structural element to separate aggregates that share a boundary. After the erosion, the internal holes of each one of the aggregates were filled, using a flood fill algorithm to fill the external area of the aggregates. From this process, voxels with 0 value were only the internal voxels of the aggregates. Then, the negative of this volume was added to the original eroded volume to fill the holes. This volume was used to label the different aggregates. An ID was assigned to each aggregate using a connected components algorithm. The labeled volume was used to obtain the pore structures in each aggregate. Each one of the labels was used to define a binary mask per aggregate, the mask was multiplied element by element with the original image volume, and the pores were all the voxels below a threshold value. The threshold value to define a pore voxel was obtained using a fuzzy c-means classification of the voxels in the masked volume. Finally, a new connected components method was applied to the final binarized volume to label each of the pores inside each aggregate. A detailed explanation of the morphological operations can be found in González and Woods (2018). Individual identifiers were assigned to each aggregate; then, the aggregate volume, the total pore volume, the total number of pores, and porosity fraction (the total pore volume divided by the containing-aggregate volume) were calculated. The pores inside each aggregate were also characterized by their volume, maximum diameter of the ellipsoid containing them, and surface

area. Only pores with at least three voxels in each direction (27 cubic voxels or 373.248 μm^3) were considered for these characterizations.

2.5.3. Morphometric analysis

To guarantee our analyses were carried out only on intact macroaggregates, we discarded all aggregates with an equivalent diameter below 250 μm (minimum volume of 8.18×10^6 μm^3). The total porosity for each pore (with the dimensions given in section 2.5.2) was calculated as the volume of the pore divided by the total pore volume in the aggregate. Then, pores were classified according to their size and form, these classifications were used as descriptors of microstructure.

The pore size distribution was calculated considering the major axis of the included ellipsoid as the equivalent pore diameter, following the Cameron and Buchan (2006) pore size classification: micropores, from 5 to 30 μm; mesopores, from 30 to 75; and macropores, from 75 to 1000 μm.

The pore form distribution was calculated as the form factor, which results from the ratio of the surface area of a sphere with the same volume as the pore to the measured surface area of the pore (Zhou et al., 2012; Pagliai et al., 2004; Prado et al., 2009), as indicated in Eq. (5).

$$F = A_e / A \tag{5}$$

Where F is the form factor, A_e (μm^2) is the area of the sphere with the same volume as the pore, and A (μm^2) is the area of the pore. The pores classes were those proposed by Ringrose-Voase (1996) with the F values of Zhou et al. (2012): channel pores ($0.5 < F < 1$), packing pores ($0.2 < F < 0.5$), and fissure pores ($F \leq 0.2$), where packing pores are those without a defined form.

A total of 12 macroaggregates in each treatment were analyzed; the individual data is given in Table S6 and S7.
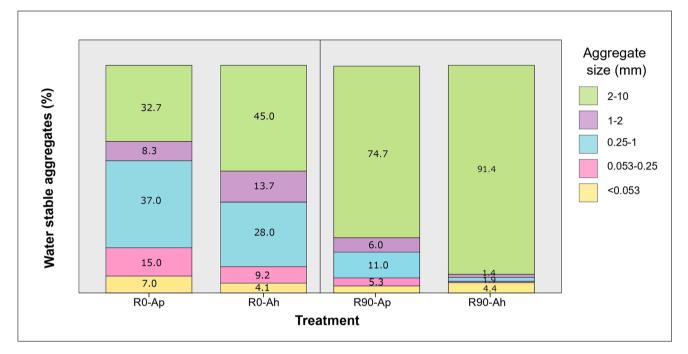
2.6. Statistical analysis

The normality of the results was verified by a Shapiro-Wilk test. Non-normal distributions were observed (Table S8 to S10), so a Kruskal-Wallis test (with an associated Games Howell test in the post hoc analysis) was performed, to analyze if there existed significant differences in physicochemical characteristics among treatments.

The Mann-Whitney U Test was performed to evaluate if long-term wastewater irrigation had any effect on the soil's physicochemical properties or macro and microstructure indicators. The Kruskal-Wallis test was used to detect significant differences in soil aggregate stability among the treatments. Finally, a Spearman correlation matrix was performed between structural indicators and physicochemical properties. For all statistical analyses, significant results were considered at $p < 0.05$ level. All the statistical analyses were conducted using IBM SPSS Statistics version 21 (SPSS, 2020). Furthermore, the effect size and statistical power were conducted with the G*power software (Faul et al., 2007).

Table 5
Mann-Whitney test for physicochemical characteristics.

	Rainfed (n = 16) Mean rank	WW-irrigated (n = 16) Mean rank	Z	U	p	1- β	d
Organic C	10.19	22.81	−3.807	27	**0.001**	0.78	1.63
Total N	9.81	23.19	−4.052	21	**0.001**	**0.86**	1.74
[Na +]	8.5	24.50	−4.826	0.001	**0.003**	**1**	4.96
EC	1.44	22.56	−3.656	31	**0.002**	0.34	1.15
pH	19.03	13.97	−1.527	87.5	0.127	0.528	0.589

Fig. 1. Aggregates distribution in the treatments (not-irrigated Ap, not irrigated Ah, irrigated Ap, and irrigated Ah). A: Mega aggregates (2–10 mm); B: Big macro aggregates (1–2 mm); C: Small macro aggregates (0.25–1 mm); D: Micro aggregates (0.053–0.25 mm); E: Mineral fraction (<0.053 mm).

Table 6
Mann-Whitney test for aggregates' distributions.

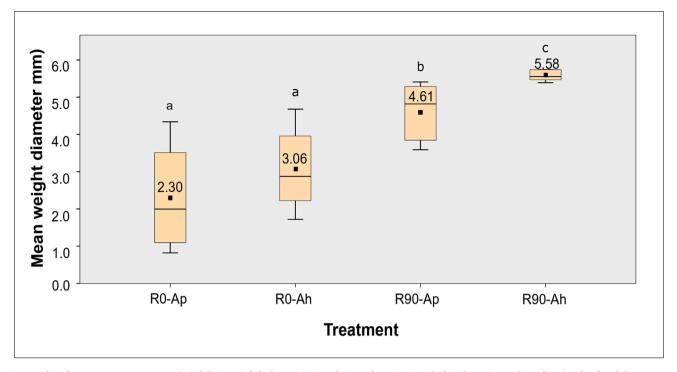|	Rainfed (n = 16) Mean rank	WW-irrigated (n = 16) Mean rank	Z	U	p	1- β	d
MWD	9.38	23.63	−4.298	14	**0.001**	**1**	2.36
A distribution	9.38	23.63	−4.297	14	**0.002**	**0.99**	2.20
B distribution	20.59	10.41	−3.675	30.5	**0.003**	0.76	1.59
C distribution	23.75	9.25	−4.373	12	**0.004**	0.95	1.98
D distribution	23.19	9.81	−4.033	21	**0.005**	0.83	1.7
E distribution	20.47	12.53	−2.395	64.5	**0.017**	0.43	0.84

3. Results and discussion

3.1. Physicochemical characteristics

The clay content, bulk density, and total porosity (of the bulk soil) were similar among all treatments (Table 2). The results of the Kruskal-Wallis test for the physicochemical properties among the groups (Table 4) showed the different treatments affected the amounts of C and N, [Na+], EC, and pH. This is consistent with previous works where soil organic matter content as well as [Na +] and EC have increased after WW irrigation (Gharaibeh et al., 2016; Mahmoud et al., 2012; Vogeler, 2009). Long-term WW- irrigated samples had significantly higher contents of C and N than rainfed samples (Table 4). The amount of C and N in the R90-Ap treatment was higher than that of both horizons in the rainfed samples; those concentrations were also higher in the R90-Ah

treatment compared to the R0-Ah treatment (but there were no statistically significant differences with the R0-Ap). The C and N content in R90-Ap treatment was significantly higher than in the R90-Ah treatment. A higher accumulation of organic matter in surficial horizons of rainfed and WW-irrigated soils has been previously observed by Gharaibeh et al. (2016).

Table 4 also shows that [Na+] was significantly higher in both horizons of long-term WW-irrigated samples than in both horizons of rainfed samples. There were no significant differences between horizons for inside a modality (WW or rainfed). The EC of both WW-irrigated horizons (R90-Ap and R90-Ah) was higher than EC in the sub-surficial rainfed samples (R0-Ah), but not in the surficial zones (R0-Ap). The pH of the R0-Ah samples was significantly higher than that of R90-Ap; this is contradictory with the findings of Gharaibeh et al. (2016) where pH was higher in WW-irrigated soils.

Fig. 2. Boxplot of MWD among treatments (rainfed Ap, rainfed Ah, WW irrigated Ap, and WW irrigated Ah). The points and numbers inside of each box represents the mean of the group. For each treatment n = 8. Different letters above the whiskers indicate significant differences (p < 0.05) among the treatments (Games-Howell post-hoc test).

Table 7
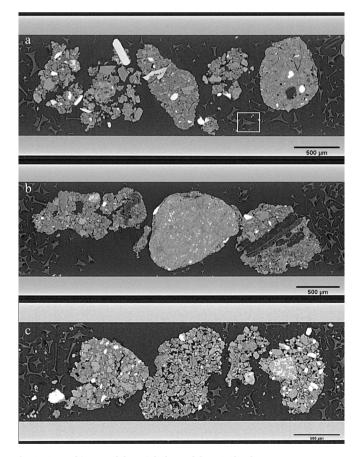Spearman correlations between mean weight diameter and physicochemical properties.

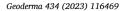| Treatment		Organic C	Total N	Na+	EC	pH
General (n = 32)	ρ^j	**0.467****	**0.476****	**0.743****	**0.496****	-0.143
	Sig	**0.007**	**0.006**	**0.001**	**0.004**	0.435
	P^k	**0.683**	**0.69**	**0.862**	**0.704**	0.378
	$1-\beta^l$	**0.635**	**0.632**	**0.918**	**0.614**	0.78
Rainfed (n = 16)	ρ	-0.066	-0.158	0.283	0.432	-0.121
	Sig	0.807	0.559	0.288	0.094	0.656
	P	0.260	0.400	0.530	0.660	0.350
	$1-\beta$	0.880	0.860	0.880	0.900	0.860
Long-term WW irrigated (n = 16)	ρ	**-0.676****	**-0.633****	−0.268	**-0.578***	0.274
	Sig	**0.004**	**0.008**	0.315	**0.019**	0.304
	P	**0.822**	**0.796**	0.518	**0.76**	0.523
	$1-\beta$	**0.914**	**0.909**	0.878	**0.91**	0.88

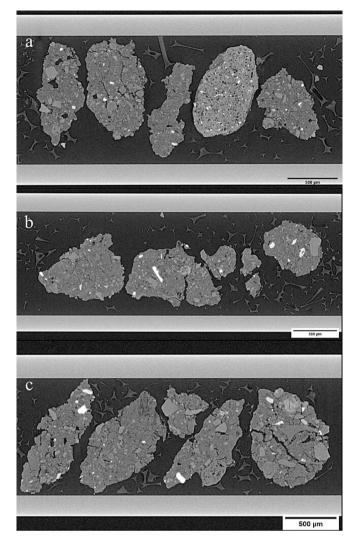[j]ρ: Spearman correlation coefficient.
[k]P: effect size.
[l]$1-\beta$:statistical power.

When analyzing whether long-term WW irrigation has any effect on soil physicochemical properties (without distinction of the horizon) it was observed that the higher values obtained for organic C, total N, EC, and [Na$^+$] in the WW-irrigated samples were significantly different from those of rainfed samples (Table 5). According to the effect size (d) given in Table 5, the higher influence of WW is observed in the Na$^+$ content followed by total N, organic C, and EC; nevertheless, according to the statistical power (1- β) only results for Na$^+$ and total N (and possibly organic C) should be considered.

Fig. 3. Central image of the axial plane of the R0-Ah scheme. Aggregates were taken from the following plots: a) R0P1, b) R0P2, and c) R0P3. The square in Fig. 3a show the foam particles form.

Fig. 4. Central image of the axial plane of the R90-Ah treatment. Aggregates were taken from the following plots: a) R90P1, b) R90P2, and c) R90P3.

3.2. Aggregates stability

The aggregate size distribution of the R0-Ap treatment was highly heterogeneous (Fig. 1), with all the studied classes represented in it. The mega aggregates (class "A", 2–10 mm) and small macro aggregates (class "C", 0.25–1 mm) classes were the most abundant (32.7% and 37% respectively). The aggregate size distribution of the R0-Ah treatment was also heterogeneous, with the "A" and "B" classes being the most abundant (45% and 14% respectively). The increase of these two classes (compared to R0-Ap) resulted in a decrease in smaller–size classes.

For the WW irrigated samples, "A" was the most abundant aggregate size class, and homogeneous distributions were observed for both horizons ("A" class abundance of 74.7% and 91.4% for treatments R90-Ap and R90-Ah, respectively). In the Ap horizon, the contribution of the smaller–size classes was about 25%, while for the Ah horizon, it only reached around 10%. Table 6 shows the statistical analysis of these long-term effects of WW irrigation on soil aggregate distribution. Soils irrigated for 90 years with WW had aggregates distributions significantly different from rainfed samples. As expected, the higher WW influence was observed for class "A" abundance, but WW influence on smaller aggregate classes reduction ("C" and "D") was also important. The statistical power shows that WW influence on the distribution of classes "B" and "E" is not generalizable.

A higher presence of class "A" aggregates than any other aggregates

class in WW irrigated soils was also observed by Mahmoud et al. (2012), who studied the influence of 5 and 15 years under olive mill WW irrigation on soil structure, while their control (freshwater) had more presence of all the studied aggregates classes. They attributed the higher mega aggregate presence to an increase in SOC.

Table 6 also shows that the main indicator of structural stability (the mean weight diameter, MWD) is also significantly different in WW long-term irrigated soils compared to rainfed soils and that WW has an important effect on structural stability. In that sense, the lowest averages for the MWD (Fig. 2) were observed for the R0-Ap treatment, while R90-Ah presented the highest; nevertheless, all the MWD values corresponded with what Bissonais (1996) reported as very stable soil structures (MWD > 2 mm).
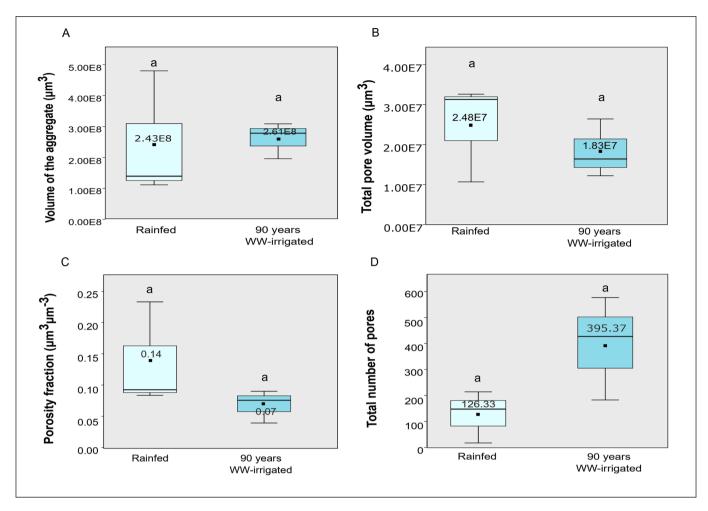
The results of the Kruskal Wallis test (Table S11) showed the effects of long-term WW irrigation and soil horizon on mean weight diameter [H(3) = 23.06, p < 0.001]. The post hoc analysis performed with the Games Howell test showed that the sub-surficial WW irrigated horizon had a higher mean weight diameter (Median = 5.56) than the surficial WW irrigated horizon (Median = 4.82p =.032) CI$_{95\%}$ [0.09, 1.85], as well as than surficial (Median = 2.00p =.001) CI$_{95\%}$ [1.68, 4.90] and sub-surficial (Median = 2.88p =.001) CI$_{95\%}$ [1.27, 3.77] rainfed horizons. The surficial WW irrigated horizon had a higher mean weight diameter than surficial (Median = 2.00p =.001) CI$_{95\%}$ [0.65, 3.99] and sub-surficial (p =.024) CI$_{95\%}$ [0.19, 2.91] rainfed horizons. There were no significant differences between the two horizons of rainfed soils.

The higher aggregate stability observed for the WW-irrigated sub-surficial horizons is partially contradictory with the observations of Gharaibeh et al. (2016) who studied the effect of 2 and 5 years of WW irrigation on aggregate stability of surficial (0–15 cm) and sub-surficial (15–30 cm) soil horizons. Although they also observed that WW-irrigated soils had greater aggregate stability than rainfed soils, the surficial horizons (with more organic matter accumulation) had greater stability. Though perhaps the organic matter accumulation is not the principal mechanism that regulates aggregate stability, the difference between our observations and those of Gharaibeh et al (2016) may exist due to tillage operations in the soils analyzed in this work.

The Spearman correlations between mean weight diameter and soil physicochemical properties (Table 7) highlight a moderate correlation with organic C ($\rho = 0.467$, p =.007), total N ($\rho = 0.476$, p =.006), EC ($\rho = 0.496$, p =.004), and [Na +] ($\rho = 0.743$, p <.001). However, these results cannot be generalized because the statistical power (1-β) only reached values of 0.614 to 0.632. When analyzing the rainfed (n = 16) and wastewater-irrigated soils (n = 16) separately, it was observed that the mean weight diameter in the rainfed soils was not correlated with any physicochemical property. However, the mean weight diameter in the WW-irrigated soils was negatively correlated with the previously indicated physicochemical properties. Nevertheless, their statistical power allows the generalization of the results between the WW-irrigated samples.

Although aggregates stability is positively correlated with Na$^+$ content (when n = 32), it is most likely that this relationship is associative rather than causal because WW-irrigated soils had both high aggregate stability and sodium content. However, it should be noted that aggregate stability was higher in the WW-irrigated soils, although the literature suggests that long-term Na$^+$ accumulation in soil should reduce aggregate stability.

It has been documented that in the long-term WW-irrigated soils of the Mezquital Valley, lignin incorporation, due to alfalfa crop residues, increases the SOC stock (Sánchez-González et al., 2017). Thus, we should include the alfalfa influence between the possible mechanisms explaining the aggregates' stability increase (despite the higher content of Na$^+$). As alfalfa crops are known for ameliorating soil structure by promoting a rapid formation of macroaggregates (Clark et al., 2009), therefore they may influence the WW-irrigated soils. This effect is not present in rainfed soils because alfalfa is not cultivated there. According to Halder et al. (2022), alfalfa residues are easily decomposed (C/N

Fig. 5. Tomography results of the microstructural pore space features for aggregates 0.5–1 mm in size from the sub surficial (Ah) horizons. The points and numbers inside of each box represents the mean of the group. For each treatment n = 3. Different letters above the whiskers indicate significant differences (p < 0.05) among the treatments (Mann-Whitney test).

ratio = 9.5), so they promote an intense initial microbial activity which leads to the secretion of extra-cellular compounds that act as temporary binding agents to form stable macro aggregates. The reported aggregate stability in this study for the WW-irrigated soils is consistent with previous reports, where alfalfa has increased the mean weight diameter by increasing the water-stable aggregates higher than 2 mm at the expense of smaller aggregate classes (corresponding in this work to the "C" class). However, the literature also refers that (in incubation experiments) initial alfalfa effects were not permanent because the decomposition of temporary binding agents disrupted the macro aggregates and broke them into smaller sizes aggregates after four weeks (Halder et al., 2022). As we did not observe a high proportion of smaller sizes aggregates in WW-irrigated soils and because alfalfa was not cultivated for at least a year before the sampling for this experiment, another mechanism different from alfalfa influence may exist.
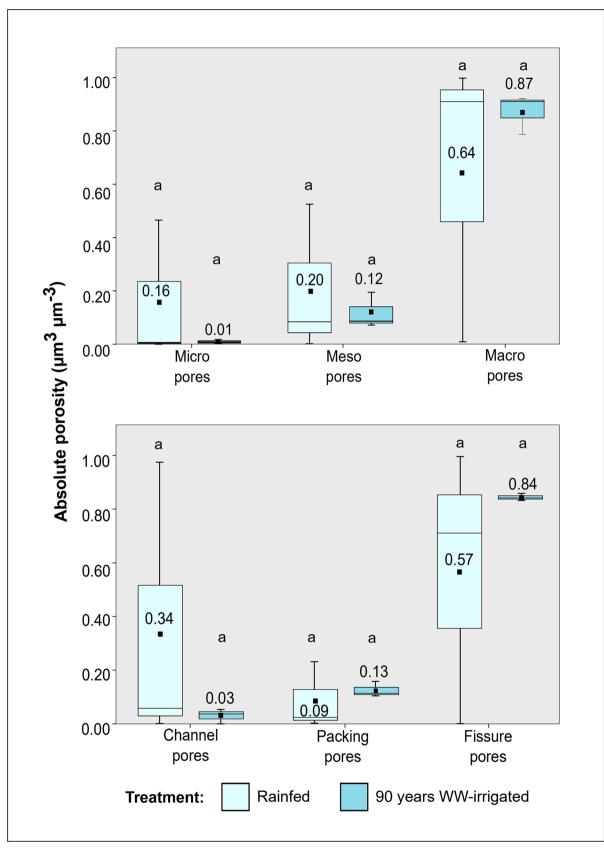
In WW-irrigated soils, the organic matter of the wastewater constitutes an easily mineralizable carbon source (from Table 1, wastewater C/N ratio = 2.10). The irrigation of the plots takes place every 28 days and irrigation can be considered a "hot moment" of microbial activity that favors soil aggregation. This continuous input of organic matter, in addition to the microbial activity resulting from the soil carbon content, which increases with the number of years under irrigation, are the factors that favor the higher structural stability in agricultural management sites that include the permanent use of the soil and the irrigation with wastewater. We suggest that microbiological activity in conjunction with structural stability should be monitored to better understand their

relationship.

WW can be considered as an organic amendment, because of the strong contribution of nutrients and highly labile organic C (Sánchez-González, 2018). In this context, it has been reported that, at the macrostructural level, SOC enhanced the stability of soil aggregate, reducing the bulk density (Naveed et al., 2014; Zhou et al., 2016; Eden et al. 2017), leading to more porous soils; although in this work a lower bulk density (and a greater total porosity) in surficial WW-irrigated horizons were observed (Table 2), there were not significative differences with the other treatments (Table 4), so our hypothesis relating organic matter accumulation with an increase in total porosity turns out to be false.

3.3. Microstructural pore space

Figs. 3 and 4 show the raw central image of the axial plane for the rainfed and WW irrigated aggregates (0.5 to 1 mm in size) respectively. In rainfed plots, highly cracked aggregates were observed, especially for aggregates coming from plot 3, and to a lesser extent for aggregates from plot 1. In WW-irrigated plots, less heterogeneity was observed, as well as a decrease in the occurrence of cracks. One can notice the presence of dense particles (white spots) and particles less dense than the aggregates themselves that may correspond to organic matter.

As shown in Fig. 5B, the total pore volume in the aggregates (volume of aggregate occupied by pores) of rainfed samples was higher than that of the WW-irrigated one, while the total number of pores was lower in

Fig. 6. Tomography results of the total porosity (classified according to the pore size and form) for aggregates 0.5–1 mm in size from the sub surficial (Ah) horizons. The points and numbers inside of each box represents the mean of the group. For each treatment n = 3. Different letters above the whiskers indicate significant differences (p < 0.05) among the treatments (Mann-Whitney test).

the former than in the latter, although these differences were not statistically significant (Table S12). Table S12 also shows that there was no significant difference in total porosity from WW-irrigated samples when compared to rainfed samples, regardless of whether the porosity was classified by size or shape without distinction if such porosity was classified according to their size or form. However, Fig. 6 shows that there was a greater dispersion in total porosity in rainfed aggregates than in WW-irrigated ones. This may explain the absence of significant differences in pore distribution between treatments. Therefore, because of this lack of significance, the differences discussed below should only be considered as descriptive features and the references to other works are only meant to compare our results to those of the literature, not to validate them.

In this study, aggregates taken from the R90-Ah samples showed a lower total pore volume (volume of aggregate occupied by pores) than rainfed samples (Figs. 5 and 6). It has been reported that the increase in SOC after 40 years of manure fertilization increased the macropores (100 – 200 μm) and decreased micropores (12.5–25 μm) at the aggregate level (Dal Ferro et al., 2013). In this research, a similar result was observed (an increase in the total number of pores in the aggregates). Furthermore, the numerically higher presence of fissure pores observed in the WW-irrigated samples (R90-Ah) is consistent with previous findings (Dal Ferro et al., 2012; Papadopoulos et al., 2009; Pagliai et al., 2004) reporting a higher pores presence in soils with organic amendments versus control or inorganic fertilization. The lack of statistical significance does not allow us to analyze whether the pore space features are correlated with physicochemical properties, but this set of findings adds, to some extent, to the knowledge relating to WW-irrigation with microstructural pore space features. The higher presence of macropores as well as the higher aggregate stability in the long-term WW-irrigated soils suggest that such parameters may be correlated (as previously hypothesized by de Gryze et al., 2006), however, to establish such a correlation a larger number of samples must be analyzed.

4. Conclusions

In this work, we analyzed the long-term (≥90 years) WW irrigation effect on soil structure by combining two different approaches: the well-documented MWD and high-resolution tomographic images, which allowed us to explore the WW irrigation effect from aggregates and pore space perspectives.

The long-term wastewater irrigated samples had a higher SOC content, as well as higher structural stability compared to rainfed soils; however, the correlation between SOC and stability was not strongly established. Instead of that, it has emerged that organic C accumulation is not the primary mechanism that regulates aggregates stability in these soils. We suggest that such stability may stem from the combined influence of crop type, WW-irrigation and intense microbial activity.

Regarding the pore space, there was no significant difference between WW-irrigated and rainfed samples (due to the high heterogeneity in the rainfed samples). Thus, correlations between microstructural pore space features and physicochemical properties could not be established. It is proposed that an analysis of a higher number of samples could help to better understand the WW irrigation effect on microstructural pore space.

Declaration of Competing Interest

The authors declare that they have no known competing financial interests or personal relationships that could have appeared to influence the work reported in this paper.

Data availability

Data will be made available on request.

Appendix A. Supplementary data

Supplementary data to this article can be found online at https://doi.org/10.1016/j.geoderma.2023.116469.

References

Abbruzzini, T.F., Reyes-Ortigoza, A.L., Alcántara-Hernández, R.J., Mora, L., Flores, L., Prado, B., 2022. Chemical, biochemical, and microbiological properties of Technosols produced from urban inorganic and organic wastes. J. Soils Sediments 22, 146–161. https://doi.org/10.1007/s11368-021-03062-2.

Almajmaie, A., Hardie, M., Acuna, T., Birch, C., 2017. Evaluation of methods for determining soil aggregate stability. Soil Tillage Res. 167, 39–45. https://doi.org/10.1016/j.still.2016.11.003.

Amézketa, E., 1999. Soil Aggregate Stability: A Review. J. Sustain. Agric. 14, 83–151. https://doi.org/10.1300/J064v14n02_08.

Bronick, C.J., Lal, R., 2005. Soil structure and management: a review. Geoderma 124, 3–22. https://doi.org/10.1016/j.geoderma.2004.03.005.

Cameron, K.C., Buchan, G.D., 2006. Porosity and pore-size distribution. In: Lal, R. (Ed.), Encyclopedia of Soil Science. Taylor and Francis, pp. 1350–1353.

Clark, G.J., Sale, P.W.G., Tang, C., 2009. Organic amendments initiate the formation and stabilisation of macroaggregates in a high clay sodic soil. Soil Res. 47, 770. https://doi.org/10.1071/SR09119.

Dal Ferro, N., Delmas, P., Duwig, C., Simonetti, G., Morari, F., 2012. Coupling X-ray microtomography and mercury intrusion porosimetry to quantify aggregate structures of a cambisol under different fertilisation treatments. Soil Tillage Res. 119, 13–21. https://doi.org/10.1016/j.still.2011.12.001.

Dal Ferro, N., Charrier, P., Morari, F., 2013. Dual-scale micro-CT assessment of soil structure in a long-term fertilization experiment. Geoderma 204–205, 84–93. https://doi.org/10.1016/j.geoderma.2013.04.012.

De Gryze, S., Jassogne, L., Six, J., Bossuyt, H., Wevers, M., Merckx, R., 2006. Pore structure changes during decomposition of fresh residue: X-ray tomography analyses. Geoderma 134, 82–96. https://doi.org/10.1016/j.geoderma.2005.09.002.

Díaz-Zorita, M., Perfect, E., Grove, J.H., 2002. Disruptive methods for assessing soil structure. Soil Tillage Res. 64, 3–22. https://doi.org/10.1016/S0167-1987(01)00254-9.

Durner, W., Iden, S.C., von Unold, G., 2017. The integral suspension pressure method (ISP) for precise particle-size analysis by gravitational sedimentation. Water Resour. Res. 53, 33–48. https://doi.org/10.1002/2016WR019830.

Duwig, C., Prado, B., Tinet, A.-J., Delmas, P., Dal Ferro, N., Vandervaere, J.P., Denis, H., Charrier, P., Gastelum Strozzi, A., Morari, F., 2019. Impacts of land use on hydrodynamic properties and pore architecture of volcanic soils from the Mexican Highlands. Soil Res. 57, 629–641. https://doi.org/10.1071/SR18271.

Eden, M., Gerke, H.H., Houot, S., 2017. Organic waste recycling in agriculture and related effects on soil water retention and plant available water: a review. Agron. Sustain. Dev. 37, 11. https://doi.org/10.1007/s13593-017-0419-9.

Elliot, E.T., Coleman, D.C., 1988. Let the Soil Work for Us. Ecol. Bull. 39, 23–32.

Faul, F., Erdfelder, E., Lang, A.-G., Buchner, A., 2007. G*Power 3: A flexible statistical power analysis program for the social, behavioral, and biomedical sciences. Behav. Res. Methods 39, 175–191. https://doi.org/10.3758/BF03193146.

Gharaibeh, M.A., Eltaif, N.I., Al-Abdullah, B., 2007. Impact of Field Application of Treated Wastewater on Hydraulic Properties of Vertisols. Water. Air. Soil Pollut. 184, 347–353. https://doi.org/10.1007/s11270-007-9423-z.

Gharaibeh, M.A., Ghezzehei, T.A., Albalasmeh, A.A., Alghzawi, M.Z., 2016. Alteration of physical and chemical characteristics of clayey soils by irrigation with treated waste water. Geoderma 276, 33–40. https://doi.org/10.1016/j.geoderma.2016.04.011.

González, R.C., Woods, R.E., 2018. Morphological Image Processing. Digital Image Processing. Pearson 635–697.

González-Méndez, B., Webster, R., Fiedler, S., Siebe, C., 2017. Changes in soil redox potential in response to flood irrigation with waste water in central Mexico. Eur. J. Soil Sci. 68, 886–896. https://doi.org/10.1111/ejss.12484.

Halder, M., Liu, S., Zhang, Z.B., Guo, Z.C., Peng, X.H., 2022. Effects of organic matter characteristics on soil aggregate turnover using rare earth oxides as tracers in a red clay soil. Geoderma 421, 115908. https://doi.org/10.1016/j.geoderma.2022.115908.

Harris, D., Horwáth, W.R., van Kessel, C., 2001. Acid fumigation of soils to remove carbonates prior to total organic carbon or CARBON-13 isotopic analysis. Soil Sci. Soc. Am. J. 65, 1853–1856. https://doi.org/10.2136/sssaj2001.1853.

Hernández-Martínez, J.L., Prado, B., Cayetano-Salazar, M., Bischoff, W.-A., Siebe, C., 2018. Ammonium-nitrate dynamics in the critical zone during single irrigation events with untreated sewage effluents. J. Soils Sediments 18, 467–480. https://doi.org/10.1007/s11368-016-1506-2.

Hettiarachchi, H., Ardakanian, R. (Eds.), 2016. Safe use of waste water in agriculture: good practice examples. UNU-Flores, Dresden, Germany.

Leuther, F., Schlüter, S., Wallach, R., Vogel, H.-J., 2019. Structure and hydraulic properties in soils under long-term irrigation with treated wastewater. Geoderma 333, 90–98. https://doi.org/10.1016/j.geoderma.2018.07.015.

Levy, G.J., Assouline, S., 2010. Physical Aspects. In: Levy, G.J., Fine, P., Bar-Tal, A. (Eds.), Treated Wastewater in Agriculture. Wiley-Blackwell, Oxford, UK, pp. 306–327. https://doi.org/10.1002/9781444328561.ch9.

Lüneberg-Rodríguez, K.C., 2018. Efecto del cambio de uso de suelo y de las prácticas de irrigación en la comunidad microbiana del suelo del Valle del Mezquital. Universidad Nacional Autónoma de México, Mexico City, Hidalgo.

Mahmoud, M., Janssen, M., Peth, S., Horn, R., Lennartz, B., 2012. Long-term impact of irrigation with olive mill wastewater on aggregate properties in the top soil. Soil Tillage Res. 124, 24–31. https://doi.org/10.1016/j.still.2012.04.002.

Marchuk, S., Marchuk, A., 2018. Effect of applied potassium concentration on clay dispersion, hydraulic conductivity, pore structure and mineralogy of two contrasting Australian soils. Soil Tillage Res. 182, 35–44. https://doi.org/10.1016/j.still.2018.04.016.

Menon, M., Mawodza, T., Rabbani, A., Blaud, A., Lair, G.J., Babaei, M., Kercheva, M., Rousseva, S., Banwart, S., 2020. Pore system characteristics of soil aggregates and their relevance to aggregate stability. Geoderma 366, 114259. https://doi.org/10.1016/j.geoderma.2020.114259.

Moritsuka, N., Izawa, G., Katsura, K., Matsui, N., 2015. Simple method for measuring soil sand content by nylon mesh sieving. Soil Sci. Plant Nutr. 61, 501–505. https://doi.org/10.1080/00380768.2015.1016864.

Müller, K., Duwig, C., Prado, B., Siebe, C., Hidalgo, C., Etchevers, J., 2012. Impact of long-term wastewater irrigation on sorption and transport of atrazine in Mexican agricultural soils. J. Environ. Sci. Heal. Part B 47, 30–41. https://doi.org/10.1080/03601234.2012.606416.

Naveed, M., Moldrup, P., Vogel, H.-Jörg., Lamandé, M., Wildenschild, D., Tuller, M., de Jonge, L.W., 2014. Impact of long-term fertilization practice on soil structure evolution. Geoderma 217-218, 181–189.

Pagliai, M., Vignozzi, N., Pellegrini, S., 2004. Soil structure and the effect of management practices. Soil Tillage Res. 79, 131–143. https://doi.org/10.1016/j.still.2004.07.002.

Papadopoulos, A., Bird, N.R.A., Whitmore, A.P., Mooney, S.J., 2009. Investigating the effects of organic and conventional management on soil aggregate stability using X-ray computed tomography. Eur. J. Soil Sci. 60, 360–368. https://doi.org/10.1111/j.1365-2389.2009.01126.x.

Pituello, C., Dal Ferro, N., Simonetti, G., Berti, A., Morari, F., 2016. Nano to macro pore structure changes induced by long-term residue management in three different soils. Agric. Ecosyst. Environ. 217, 49–58. https://doi.org/10.1016/j.agee.2015.10.029.

Prado, B., Duwig, C., Márquez, J., Delmas, P., Morales, P., James, J., Etchevers, J., 2009. Image processing-based study of soil porosity and its effect on water movement through Andosol intact columns. Agric. Water Manag. 96, 1377–1386. https://doi.org/10.1016/j.agwat.2009.04.012.

Prado, B., Strozzi, A.G., Huerta, E., Duwig, C., Zamora, O., Delmas, P., Casasola, D., Márquez, J., 2016. 2,4-D mobility in clay soils: Impact of macrofauna abundance on soil porosity. Geoderma 279, 87–96. https://doi.org/10.1016/j.geoderma.2016.06.007.

Ringrose-Voase, A.J., 1996. Measurement of soil macropore geometry by image analysis of sections through impregnated soil. Plant Soil 183, 27–47. https://doi.org/10.1007/BF02185563.

Sánchez-González, A., 2018. Materia orgánica y su interacción con superficies minerales en suelos del Valle del Mezquital. Universidad Nacional Autónoma de México, Mexico City.

Sánchez-González, A., Chapela-Lara, M., Germán-Venegas, E., Fuentes-García, R., del Río-Portilla, F., Siebe, C., 2017. Changes in quality and quantity of soil organic matter stocks resulting from wastewater irrigation in formerly forested land. Geoderma 306, 99–107. https://doi.org/10.1016/j.geoderma.2017.07.009.

Schacht, K., Marschner, B., 2015. Treated wastewater irrigation effects on soil hydraulic conductivity and aggregate stability of loamy soils in Israel. J. Hydrol. Hydromechanics 63, 47–54. https://doi.org/10.1515/johh-2015-0010.

Schlüter, S., Sammartino, S., Koestel, J., 2020. Exploring the relationship between soil structure and soil functions via pore-scale imaging. Geoderma 370, 114370. https://doi.org/10.1016/j.geoderma.2020.114370.

Siebe, C., Chapela-Lara, M., Cayetano-Salazar, M., Prado, B., Siemens, J., 2016. Effects of More Than 100 Years of Irrigation with Mexico City's Wastewater in the Mezquital Valley. In: Hettiarachchi, H., Ardakanian, R. (Eds.), Safe Use of Waste Water in Agriculture: Good Practice Examples. UNU-Flores, Dresden, Germany, pp. 121–138.

Valipour Mohammadand Singh, V.P., 2016. Global Experiences on Wastewater Irrigation: Challenges and Prospects, in: Maheshwari Basantant Thoradeniya, B. and S.V.P. (Ed.), Balanced Urban Development: Options and Strategies for Liveable Cities. Springer International Publishing, Cham, pp. 289–327. doi: 10.1007/978-3-319-28112-4_18.

Vogeler, I., 2009. Effect of Long-term Wastewater Application on Physical Soil Properties. Water. Air. Soil Pollut. 196, 385–392. https://doi.org/10.1007/s11270-008-9785-x.

Wang, W., Kravchenko, A.N., Smucker, A.J.M., Liang, W., Rivers, M.L., 2012. Intra-aggregate Pore Characteristics: X-ray Computed Microtomography Analysis. Soil Sci. Soc. Am. J. 76, 1159–1171. https://doi.org/10.2136/sssaj2011.0281.

Wildenschild, D., Sheppard, A.P., 2013. X-ray imaging and analysis techniques for quantifying pore-scale structure and processes in subsurface porous medium systems. Adv. Water Resour. 51, 217–246. https://doi.org/10.1016/j.advwatres.2012.07.018.

Zhao, Y., Hu, X., Li, X., 2020. Analysis of the intra-aggregate pore structures in three soil types using X-ray computed tomography. CATENA 193, 104622. https://doi.org/10.1016/j.catena.2020.104622.

Zhou, H., Peng, X., Peth, S., Xiao, T.Q., 2012. Effects of vegetation restoration on soil aggregate microstructure quantified with synchrotron-based micro-computed tomography. Soil Tillage Res. 124, 17–23. https://doi.org/10.1016/j.still.2012.04.006.

Zhou, H., Fang, H., Mooney, S.J., Peng, X., 2016. Effects of long-term inorganic and organic fertilizations on the soil micro and macro structures of rice paddies. Geoderma 266, 66–74. https://doi.org/10.1016/j.geoderma.2015.12.007.